Molecular Beam Epitaxial Growth and Characterization of Cd-Based II-VI Wide-Bandgap Compounds on Si Substrates

G. BRILL,[1,3] Y. CHEN,[1] P.M. AMIRTHARAJ,[1] W. SARNEY, D. CHANDLER-HOROWITZ,[2] and N.K. DHAR[1]

1.—Sensors and Electron Devices Directorate, U.S. Army Research Laboratory, Adelphi, MD 20783. 2.—Semiconductor Electronics Division, National Institute of Standards and Technology, Gaithersburg, MD 20899. 3.—E-mail: gbrill@arl.army.mil

We have carried out a detailed study on the growth of Cd-based II-VI compounds on Si substrates using molecular beam epitaxy (MBE). CdTe, CdSe, CdSeTe, and CdZnSeTe layers were nucleated and grown on Si(211) substrates in order to study a broad range of semiconductor properties, such as crystal structure, fundamental bandgap, surface morphology, and defect and dislocation density as a function of the constituent elements. For structural characterization, we used transmission electron microscopy (TEM) and x-ray diffraction, which indicated that cubic $Cd_{1-x}Se_xTe$ material had been grown on Si substrates throughout the entire composition range. Likewise, photoreflectance (PR) and photoluminescence (PL) were used to measure the optical response in the near bandgap (E_g) region. Results indicated nonrandom ordering of CdSeTe/Si material. Studies on quaternary CdZnSeTe material indicated that Zn and Se concentrations directly impact surface morphology with extremely smooth surfaces obtained as Zn content is decreased.

Key words: CdSeTe, CdSe, CdZnSeTe, Si, (211), molecular beam epitaxy (MBE), photoluminescence (PL), photoreflectance (PR), zincblende, wurtzite, cubic, quaternary, ternary, transmission electron microscopy (TEM), bandgap, defects, bowing

INTRODUCTION

Cadmium and zinc based II–VI wide-bandgap compound semiconductors have potential applications for various opto-electronic devices as well as x-ray and γ-ray detectors.[1–4] These compounds, especially Zn-based compounds, were initially grown on GaAs substrates to mitigate issues related to the lattice mismatch between the epilayer and the underlying substrate. However, the most desirable situation is to grow high-quality Cd- and Zn-based II-VI wide-bandgap compound semiconductors directly on Si substrates to take advantage of mature Si technology for electronic processing. In addition to applications such as opto-electronic devices and x-ray/γ-ray detectors, Cd-based binary compounds grown on Si, such as CdTe/Si, have been used as composite substrates for HgCdTe material, an infrared (IR) detecting semiconductor system.[5–10]

Similarly, ternary alloys, such as CdZnTe/Si and CdSeTe/Si, as well as quaternary compounds, such as CdZnSeTe/Si, can also be used as composite substrates specifically engineered for exact lattice matching with HgCdTe material designed to detect in the long wavelength (8–12 μm) IR region through careful control of the Se or Zn concentration. Growth of such materials with appropriate quality is expected to minimize dislocations generated at the HgCdTe epilayer-composite substrate interface by eliminating lattice mismatch. Furthermore, additional applications for Cd-based and Zn-based II-VI compounds can be envisioned through the use of sophisticated device architectures encompassing quantum wells, strained layer growth, superlattices, or other novel structures throughout the entire composition range of $Cd_{1-y}Zn_ySe_xTe_{1-x}$ if the cubic crystal structure can be maintained.

(Received August 12, 2004; accepted December 22, 2004)

EXPERIMENTAL

All Cd-based II–VI materials for this study were grown on Si(211) nominal substrates in a 3-in. molecular beam epitaxy (MBE) system from DCA instruments (Turku, Finland). Since the initial motivation for this effort was to study Cd(Zn,Se)Te/Si for use as composite substrates for HgCdTe IR material growth, Si(211) substrates were chosen since this is the preferred orientation for HgCdTe material grown by MBE. The MBE system was equipped with binary CdTe and ZnTe effusion sources along with elemental Se, Cd, and As sources. The Si substrates were cleaned using the modified RCA process[11] after which a thermal cleaning process within the MBE growth chamber was executed to remove the chemically grown oxide layer. Arsenic was then used to passivate the clean Si surface after which material nucleation and growth occurred. Further details of the layer structure and growth processes have been described elsewhere.[12–14] $CdSe_xTe_{1-x}$ was grown with $0 \leq x \leq 1$ to study the fundamental bandgap and material properties as a function of Se content. $Cd_{1-y}Zn_ySe_xTe_{1-x}$ layers were grown with $x + y$ kept near 0.04 in order to study the role of Zn and Se incorporation on material properties while maintaining an overall constant lattice parameter. Additionally, optical measurements were conducted on a set of these quaternary layers. Finally, both CdTe and CdSe layers were grown to establish baseline parameters and properties.

Structural characterization was conducted using both x-ray diffraction and transmission electron microscopy (TEM). The full-width at half-maximum (FWHM) taken from double crystal rocking curve measurements of the {422} diffraction peaks from the Cd-based II–VI layers were measured to assess the general crystalline quality of the material. The x-ray diffraction system used for these studies is not well suited to determine exact lattice constants of the ternary or quaternary materials grown and hence no characterization of any residual strain present in the material can be determined at this point. However, x-ray diffraction was capable of determining the overall composition of the ternary and quaternary layers with respect to CdTe, while wavelength dispersive x-ray analysis was used to determine the individual concentrations of Zn and Se incorporated within quaternary layers.[14] The material's crystal structure was examined using TEM diffraction patterns, and high-resolution cross-sectional images were obtained with a JEOL 2010F TEM operated at 200 keV (JEOL, Tokyo). Finally, optical microscopy was used to observe surface morphology and defect density as a function of layer composition.

Optical measurements were also carried out using room-temperature photoluminescence (PL) and photoreflectance (PR) to measure the response in the near bandgap (E_g) region. Measurements were taken on both $CdSe_xTe_{1-x}$ with x ranging from 0 to unity and on $Cd_{1-y}Zn_ySe_xTe_{1-x}$ with $x + y = 0.04$, but with x and y individually varying between 0 and 0.04. The PR spectra were acquired using a Semiconductor Characterization Instruments' automated PR system.*[15,16] Spectra were recorded over the near bandgap region extending from 1 eV to ~1.9 eV with a spectral resolution of 1 meV. The pump source was a 442-nm line derived from a He-Cd laser with an average power density of the pump source at the sample surface of ~5 mW/cm^2. The detector was a thermoelectrically cooled InGaAs photodiode. The PL measurements were performed at room temperature using a conventional system comprised of a laser excitation (Kr^+, 647.1-nm line), a monochromator, and a Si detector. All optical measurements were performed at the National Institute of Standards and Technology (NIST).

RESULTS AND DISCUSSION

CdSeTe/Si Properties

Incorporation of Se into the CdTe matrix was investigated by growing $CdSe_xTe_{1-x}$ throughout the entire composition range ($0 \leq x \leq 1$). Optimal MBE growth conditions were established for low Se ($x < 0.05$) CdSeTe material growth with subsequent characterization suggesting very high-quality material had been obtained.[12,13] X-ray diffraction FWHM data from the CdSeTe layers (~5 μm thick) on average measured 125 arcsec with a low value of 97 arcsec obtained. Additionally, layers exhibited a smooth surface morphology with a low level of surface defects, typically less than 500 cm^{-2}. Lateral uniformity was also determined to be excellent across the entire 3-in. wafer.[13] It should be noted that all CdSeTe layers nucleated with $x \leq 0.05$ grew in the cubic crystal phase as determined by the presence of the {422} x-ray diffraction peak. Using these same growth conditions, $CdSe_xTe_{1-x}$ layers were grown with x increasing to unity. Since the CdTe binary compound is a zincblende crystal while the CdSe binary compound is a wurtzite crystal, it is not unreasonable to expect a phase change in crystal structure at some Se composition within the $CdSe_xTe_{1-x}$ material system as we go from CdTe ($x = 0$) to CdSe ($x = 1$). This has been reported for $CdSe_xTe_{1-x}$ grown on glass substrates with zincblende material nucleated for $x < 0.60$ and wurtzite material nucleated for $x > 0.60$.[17] Similarly, Bridgman grown bulk $CdSe_xTe_{1-x}$ was found to nucleate as zincblende for $x \leq 0.45$ and as wurtzite for $x \geq 0.65$ with a mixed phase for $0.45 \leq x \leq 0.65$.[18] However, our observation of the {422} x-ray diffraction peak clearly indicated that $CdSe_xTe_{1-x}$ remained in the cubic phase throughout the entire composition range for the MBE growth conditions used in this study. CdSe has

* Certain commercial products are identified in the manuscript to adequately specify the procedure. This does not imply recommendation or an endorsement, nor does it imply that they are the best available for the purpose.

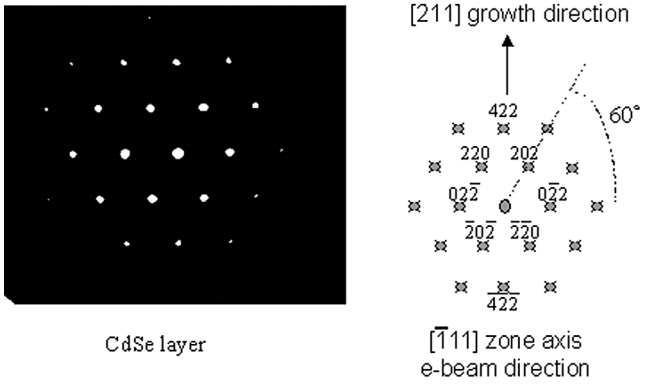

Fig. 1. TEM diffraction pattern from a CdSe layer grown on Si substrate. The diffraction pattern matches the expected pattern from a zincblende crystal viewed along the [−1 1 1] zone axis.

been reported to grow in the cubic phase on GaAs[19,20] and ZnSe[21] substrates, but this is the first reported observation of cubic $CdSe_xTe_{1-x}$ material grown throughout the entire composition range. Electron diffraction patterns along orthogonal zone axes [1 −1 0] and [−1 1 1] were also taken with the TEM system to further confirm that high Se content CdSeTe layers were cubic. Figure 1 shows the TEM diffraction pattern from a CdSe layer grown on a Si(211) substrate. Included in the figure is the expected diffraction pattern from a cubic crystal. Although twinned, similar TEM diffraction patterns were observed for $CdSe_xTe_{1-x}$ with x = 0.75 and x = 0.91 confirming zincblende material growth. The cubic structure may be favored throughout the entire composition range due to the coherency induced by the underlying cubic substrate and cubic buffer layers with the constituents of the alloy. Since the coherency from the buffer layer can accommodate local strain, it is possible that phase separation is suppressed in exchange of extended defects and hence cubic CdSeTe material is maintained even at high Se concentrations. It should also be noted that since growth was optimized for low x-value CdSeTe material, the presence of twins in high x-value CdSeTe material is not surprising. It is expected that further optimization of the growth conditions for high Se content layers will mitigate twin nucleation within the material.

Room-temperature PL and PR measurements were also made on these layers to determine the bandgap as a function of Se concentration. Figure 2 shows typical PL and PR data taken at room temperature. Intense luminescence and PR data with good signal-to-noise ratio were readily obtained from the CdSeTe layers with identification of the bandgap made simply from the position of the main spectral feature. A clear shift in the bandgap with respect to CdTe is observed dependent on the alloy composition. Figure 3 shows the bandgap data as a function of alloy composition. From the data, a large bowing factor is observed for CdSeTe material. Using a quadratic fit of the data while holding the endpoints fixed, the bowing factor, b_g (eV) = 0.996 ± 0.004, is obtained. This value fits with reported results of the CdSeTe bowing factor of 0.90[22] and 0.94,[23] which were determined from $Cd_{1-x}Se_xTe$ layers with $x \leq 0.5$. The large bowing factor has been attributed to local ordering or formation of clusters in the CdSeTe alloy. Poon et al. have shown that a AuCu-I-like structure with 67% relaxation of the alloy will account for the large bowing factor found in CdSeTe material.[22] Our results further support this conclusion based on our experimentally determined value of the CdSeTe bowing parameter. It is suggested that the large bowing factor can be explained by the local ordering of the constituent binaries in the CdSeTe wherein an "internal strain" is developed due to local Cd-Te and Cd-Se bond alterations. Figure 3b shows the bandgap dependence on x for low Se incorporation ($x \leq 0.15$), the composition range of technological interest for HgCdTe. In this region, the variation shows a linear dependence

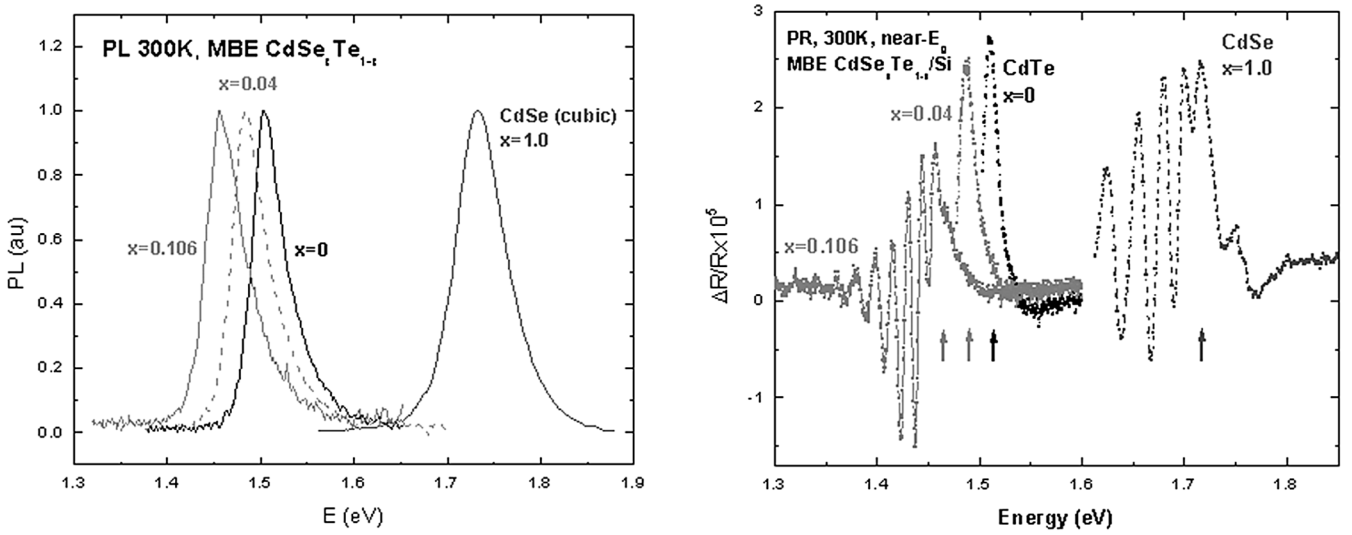

Fig. 2. Typical room-temperature PL and PR spectra taken from CdSeTe/Si material.

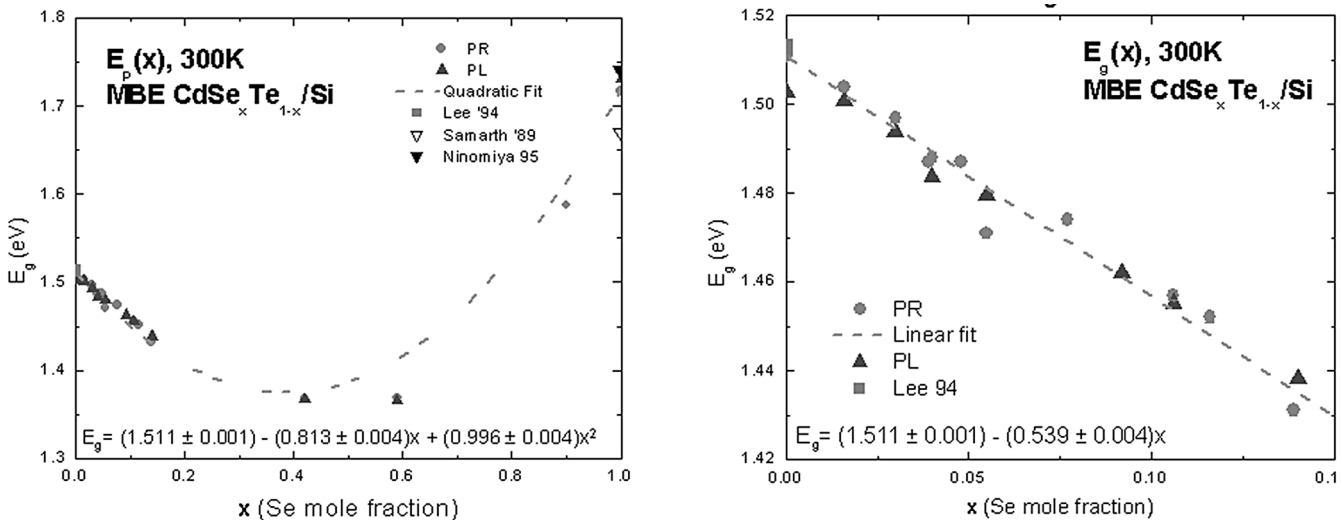

Fig. 3. $CdSe_xTe_{1-x}$ bandgap values as a function of Se composition. Included in the figures are the empirically derived equations for the bandgap. For reference, previous published values of E_g for CdTe[27] and cubic CdSe[19,28] have been included.

and can be fit with the equation $E_g(eV) = (1.511 \pm 0.001) - (0.539 \pm 0.004)x$.

CdZnSeTe/Si Properties

To study the role of anion mixing versus cation mixing within the CdTe matrix, $Cd_{1-y}Zn_ySe_xTe_{1-x}$ layers were nucleated and grown on Si substrates. The total goal composition (x + y) was kept constant near 0.04, while the constituent Zn and Se elements were varied individually approximately between 0 and 0.04. X-ray diffraction measurements were made on the set of $Cd_{1-y}Zn_ySe_xTe_{1-x}$ layers, including ternary CdSeTe (y = 0) and ternary CdZnTe (x = 0). Results indicated no significant degradation of the crystalline quality with the incorporation of both Zn and Se, regardless of the individual constituent percentages. For ternary $CdSe_xTe_{1-x}$ ($0 < x \leq 0.05$), the average FWHM value measured from 54 layers was 125 arcsec with a standard deviation of 15 arcsec. Likewise for ternary $Cd_{1-y}Zn_yTe$ ($0 < y \leq 0.05$), the average FWHM value measured from 11 layers was 110 arcsec with a standard deviation of 12 arcsec. X-ray data taken from 12 $Cd_{1-y}Zn_ySe_xTe_{1-x}$ layers ($0 \leq x + y \leq 0.05$) resulted in an average FWHM value of 118 arcsec with a standard deviation of 19 arcsec. These results are consistent with one another and indicate high-quality material growth.

However, the surface morphology of CdZnSeTe material shows a clear dependence on the level of Zn or Se incorporated into the layer. Although all quaternary layers appeared specular to the un-aided eye, under high magnification, obvious differences in the surface morphology were observed. Figure 4 shows several optical microscopy images taken from CdZnSeTe layers as a function of both Zn and Se. As seen in the figure, the CdZnTe surface exhibits roughness even though the layer was grown near the optimal MBE conditions and had excellent x-ray FWHM data. However, as the Zn content is decreased and the Se content is subsequently increased, the surface roughness decreases substantially. For ternary CdSeTe, the surface is completely smooth and mimics that of the CdTe as-grown surface. All of these layers were nucleated under identical growth conditions, which are considered to be nearly optimal for these compositions given the excellent x-ray FWHM obtained regardless of Zn or Se content. Based on these x-ray results, along with the fact that Cd-based II-VI compounds have a relatively large temperature window for quality growth, it is concluded that the improvement in surface morphology is a result of anion mixing instead of cation mixing within the CdTe matrix and not due to any needed adjustment in the growth conditions to compensate for the change in elemental mixing (i.e., Se versus Zn incorporation). This result suggests that a different epilayer surface chemistry exists during growth for anion versus cation mixed Cd-based II–VI alloys. Thus, it is likely that the differences in the binding energies[24] between the binary compounds in anion (CdTe, CdSe) and cation (CdTe, ZnTe) mixed alloys lead to the observed differences in surface morphology. However, further optimization of growth parameters could lead to better surface morphologies for all CdZnSeTe alloys studied, although it is expected that the overall surface morphology for anion mixed layers will remain superior based on these initial studies.

The dislocation density of the CdZnSeTe material was also determined through use of the Everson etch, which is known to reveal dislocations within CdTe and CdZnTe (211) orientated material.[25] Results indicate that when either "Zn-rich" ($Se < 0.01$ and $Zn > 0.03$) or "Se-rich" ($Zn < 0.01$ and $Se > 0.03$) $Cd_{1-y}Zn_ySe_xTe_{1-x}$ material was studied, the dislocation density was significantly lower than "evenly mixed" ($Se \sim 0.02$ and $Zn \sim 0.02$) $Cd_{1-y}Zn_ySe_xTe_{1-x}$ material, with an average value near 2×10^5 cm^{-2} versus an average value near 1.5×10^6 cm^{-2}, respectively. Additionally, the drop in dislocation density is independent of whether Se or Zn is reduced, although CdSeTe/Si had

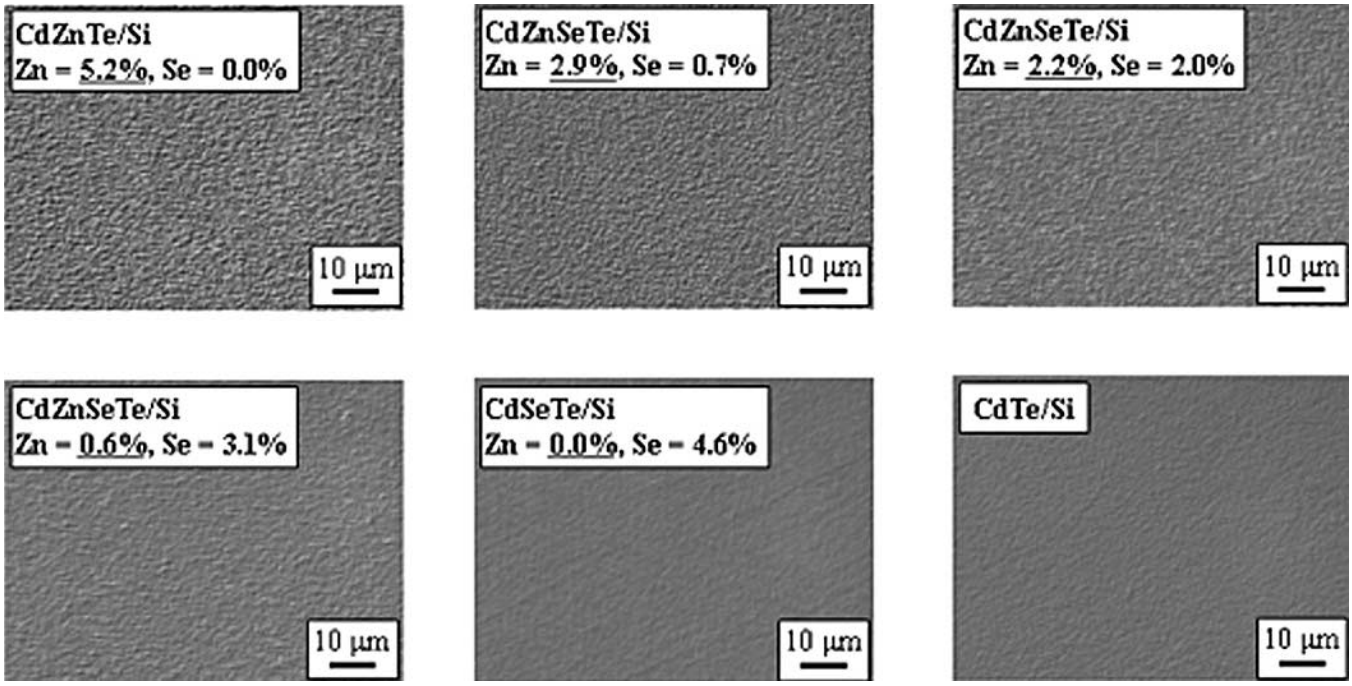

Fig. 4. Optical microscopy images of CdZnSeTe/Si layers as a function of Zn and Se incorporation. Note that the surface becomes smoother as Zn content decreases and Se increases.

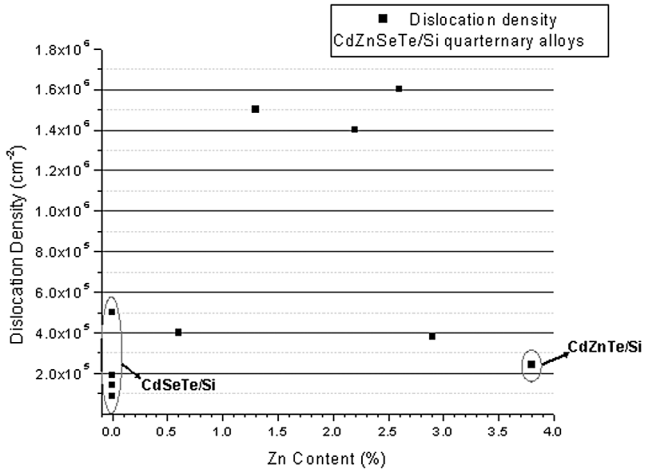

Fig. 5. Dislocation density of quaternary $Cd_{1-y}Zn_ySe_xTe_{1-x}$ material grown on Si substrates as a function of Zn content. Note that as the Zn content increases, the Se content decreases to maintain an overall composition (x + y) near 0.04.

a lower dislocation density than CdZnTe/Si, 1×10^5 cm^{-2} and 3×10^5 cm^{-2}, respectively. Figure 5 displays the dislocation density of quaternary CdZnSeTe/Si as a function of Zn and Se content.

Further characterization was carried out with room-temperature PL and PR to study the near bandgap region of the quaternary layers. Figure 6 shows typical PL and PR data, respectively, from CdZnSeTe layers. From the optical data, the bandgap energy is observed to shift dependent on the individual amount of Zn and Se incorporated even though the total composition (x + y) for these layers was kept near 0.04. Note that the PL spectra are organized in pairs to highlight this effect. When more Se is incorporated within the quaternary system with respect to Zn, the bandgap shifts to lower energies. In contrast, for "Zn-rich" material the bandgap shifts to higher energies. From our work conducted on $CdSe_xTe_{1-x}$ (Fig. 3), we fit the energy shift for low x as

$$E_g(x) = 1.511 - 0.54x \qquad (x \leq 0.15) \qquad (1)$$

From the literature,[22] the $Cd_{1-y}Zn_yTe$ bandgap energy shift for low y can be written as follows, if the quadratic term is dropped:

$$E_g(y) = 1.511 + 0.6y \qquad (y \leq 0.10) \qquad (2)$$

Since the quaternary layers under investigation in this work were grown with both low Zn and Se composition, we can combine Eqs. 1 and 2 to obtain the following expression for the bandgap shift for quaternary $Cd_{1-y}Zn_ySe_xTe_{1-x}$ layers. In units of electron volts (eV), the resulting equation is

$$E_g(x,y) = 1.511 - 0.54x + 0.6y \quad (x,y \leq 0.10) \qquad (3)$$

From this result, it is seen that Zn (y value) and Se (x value) shift the bandgap energy from the binary CdTe position nearly equal amounts but in opposite directions. This has been experimentally observed in our PL data (Fig. 6), which shows the peak from the quaternary layer with 2.2% Zn and 2.0% Se incorporated falling directly on top of the peak from the CdTe reference layer. This information further distinguishes the different growth mechanisms of cation- and anion-mixed Cd-based II-VI material. This also indicates that the lattice constant and bandgap can be controlled independently for quaternary CdZnSeTe material.

Also note that the PL spectra from higher Zn content quaternary layers shows a higher background

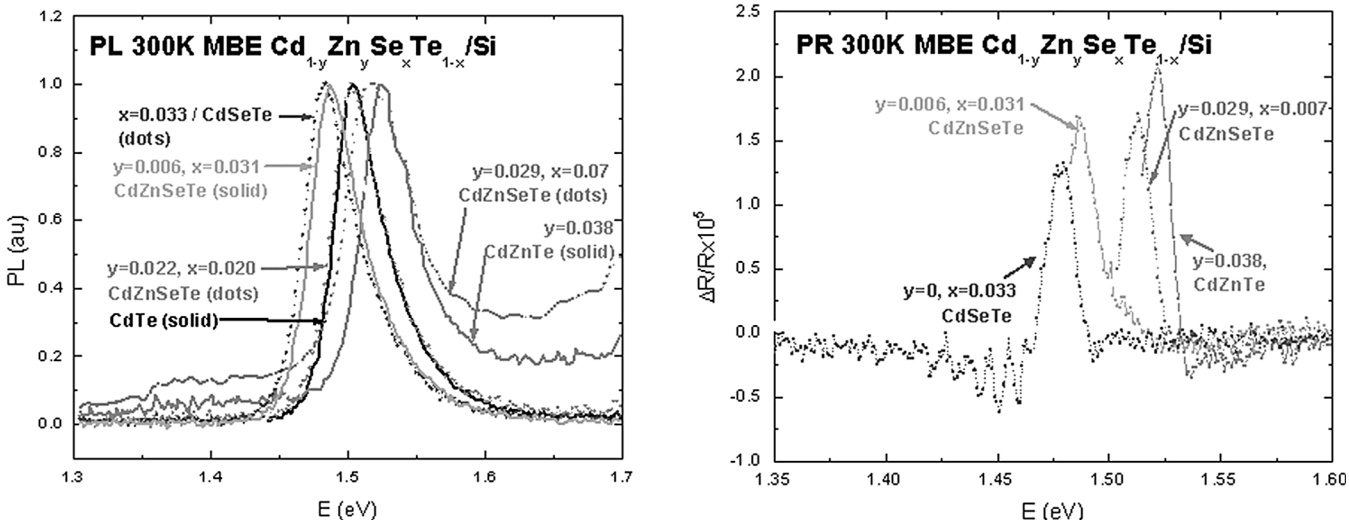

Fig. 6. Room-temperature PL and PR spectra taken from CdZnSeTe/Si material. The higher bandgap PR spectra have been truncated at the lower energies for clarity.

level. This generally indicates scattering from a rough surface. This also fits with our observation that "Se-rich" quaternary layers have a much smoother surface morphology than "Zn-rich" layers.

Figure 7 shows room-temperature PR spectra from two quaternary layers. The PR spectra are similar to those seen from high-quality bulk samples with a distinct two-lobe feature in the vicinity of the bandgap, followed by a large number of oscillatory features at lower energies. A spectrum from a CdTe epilayer is also included for comparison. For these spectra, we used the well-known Aspnes' three-point fit method to establish the bandgap values.[26] We believe the near-E_g line shape is due to a significant contribution from the excitonic component, which is an indication of the high crystalline quality. The lower energy oscillations are due to interference fringes caused as a result of the large mismatch between the optical indices of the Si substrate and the epitaxial films.

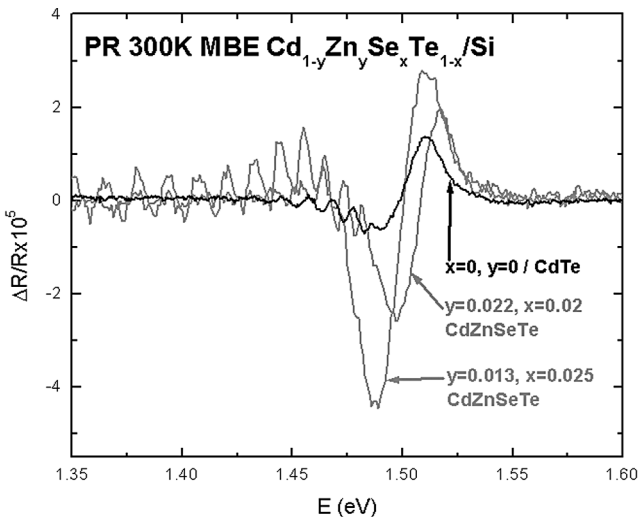

Fig. 7. Room-temperature PR spectra from select CdZnSeTe/Si layers showing excitonic behavior.

The presence of these fringes also attests to a uniform film with smooth and parallel interfaces, again an indication of high-quality films. These results warrant further investigation at lower temperatures, which will be the subject of future work.

CONCLUSIONS

We have demonstrated high-quality ternary and quaternary Cd-based II–VI growth using MBE on Si substrates. $CdSe_xTe_{1-x}$ has been demonstrated for the first time to remain in the cubic crystal phase throughout the entire range of Se compositions ($0 \leq x \leq 1$). Additionally, PL and PR optical experiments were conducted to study the optical response in the near bandgap region. Results indicated a large bowing of the bandgap as a function of composition, which suggests a nonrandom ordering of the crystal. Quaternary CdZnSeTe material properties were observed to be dependent on both Se and Zn content. Surface smoothness increased as the Se incorporation increased and the Zn incorporation decreased. The dislocation density of the material was observed to reach minimum values for either the case of low-Se/high-Zn content or low-Zn/high-Se content. Additionally, optical measurements made on these layers indicated that respective Zn and Se incorporation shifts the quaternary bandgap away from the CdTe bandgap in nearly equal amounts but in opposite directions.

REFERENCES

1. P.J. Sebastian and V. Sivaramakrishnan, *Phys. Rev. B.* 40, 9767 (1989).
2. N. Matsumura, T. Sakamoto, and J. Saraie, *J. Cryst. Growth* 251, 602 (2003).
3. D. Noda, T. Aoki, Y. Nakanishi, and Y. Hatanaka, *J. Cryst. Growth* 214–215, 1121 (2000).
4. Z.C. Feng, P. Becla, L.S. Kim, S. Perkowitz, Y.P. Feng, H.C. Poon, K.P. Williams, and G.D. Pitt, *J. Cryst. Growth* 138, 239 (1994).
5. Y.P. Chen, S. Sivananthan, and J.P. Faurie, *J. Electron. Mater.* 22, 1306 (1993).

6. W.-S. Wang and I. Bhat, *J. Electron. Mater.* 24, 451(1995).
7. T.J. deLyon, S.M. Johnson, C.A. Cockrum, O.K. Wu, W.J. Hamilton, and G.S. Kamath, *J. Electrochem. Soc.* 141, 2366 (1994).
8. P.S. Wijewarnasuriya, M. Zandian, D.D. Edwall, W.V. McLevige, C.A. Chen, J.G. Pasko, G. Hildebrandt, A.C. Chen, J.M. Arias, A.I. D'Souza, S. Rujirawat, and S. Sivananthan, *J. Electron. Mater.* 27, 546 (1998).
9. G. Brill, S. Velicu, P. Boieriu, Y. Chen, N.K. Dhar, T.S. Lee, Y. Selamet, and S. Sivananthan, *J. Electron. Mater.* 30, 717 (2001).
10. N.K. Dhar, C.E.C. Wood, A. Gray, H.Y. Wei, L. Salamanca-Riba, and J.H. Dinan, *J. Vac. Sci. Technol. B* 14, 2366 (1996).
11. W. Kern and D.A. Puotinen, *RCA Rev.* 31, 187 (1990).
12. Y.P. Chen, G. Brill, and N.K. Dhar, *J. Cryst. Growth* 252, 270 (2003).
13. Y.P. Chen, G. Brill, and N.K. Dhar, *J. Electron. Mater.* 32, 723 (2003).
14. Y.P. Chen, G. Brill, E.M. Campo, T. Hierl, J.C.M. Hwang, and N.K. Dhar, *J. Electron Mater.* 33, 498 (2004).
15. Semiconductor Characterization Instruments, Inc., Brooklyn, NY 11201.
16. F.H. Pollak, in *Handbook on Semiconductors: Optical Properties of Semiconductors,* ed. M. Balkanski (Amsterdam: North-Holland, 1994), vol. 2, p. 527.
17. P.J. Sebastian and V. Sivaramakrishnan, *J. Cryst. Growth* 112, 421 (1991).
18. M. Schenk and C. Silber, *J. Mater. Sci.: Mater. Electron.* 9, 295 (1998).
19. N. Samarth, H. Luo, J.K. Furdyna, S.B. Qadri, Y.R. Lee, A.K. Ramdas, and N. Otsuka, *Appl. Phys. Lett.* 54, 2680 (1989).
20. N. Matsumura, J. Ueda, and J. Saraie, *Jpn. J. Appl. Phys.* 39, L1026 (2000).
21. O. de Melo, C. Vargas-Hernandez, and I. Hernandez-Calderon, *Appl. Phys. Lett.* 82, 43 (2003).
22. H.C. Poon, Z.C. Feng, Y.P. Feng, and M.F. Li, *J. Phys. Condens. Matter.* 7, 2783 (1995).
23. L.V. Prytkina, V.V. Volkow, A.N. Vanyukow, and P.S. Kireev, *Sov. Phys.-Semicond.* 2, 509 (1968).
24. M. Albrecht, B. Paulus, and H. Stoll, *Phys. Rev. B.* 56, 7339 (1997).
25. W.J. Everson, C.K. Ard, J.L. Sepich, B.E. Dean, and G.T. Neugebauer, *J. Electron. Mater.* 24, 505 (1995).
26. D.E. Aspnes, in *Handbook on Semiconductors Optical Properties of Solids,* ed. M. Balkanski (Amsterdam: North Holland, 1980), vol. 2, p. 109.
27. J. Lee, N.C. Giles, D. Rajavel, and C.J. Summers, *Phys. Rev. B,* 49, 1668 (1994).
28. S. Ninomiya and S. Adachi, *J. Appl. Phys.* 78, 4681 (1995).